Structure Maps for Intermetallic Phases Using Second Moment Scaling Theory

Laura M. Hoistad[†]

Willard H. Dow Chemistry Laboratory, University of Michigan, Ann Arbor, Michigan 48109-1055

Received June 28, 1994[⊗]

Second moment scaled Hückel energies have been used to construct structure maps of intermetallic compounds with the stoichiometries ZA_3 and ZA_6. Z is an electropositive element from groups I−V or a lanthanide, and A is a late transition metal or main group element. The calculations were performed only on the covalent network of the A atoms. These structure maps plot the differences of the total energy as a function of electrons per atom for the stoichiometries above. With the use of only the covalent energy of the A network, these maps correctly demarcate the zones of stability exhibited for the structure types of $AuCu_3$, $TiNi_3$, $TiCu_3$, BiF_3, $SnNi_3$, $NdTe_3$, TiS_3, $SmAu_6$, $CeCu_6$, and $PuGa_6$. Some of these results are explained by means of a moments analysis.

Introduction

The structures of binary intermetallic compounds are very diverse. They range from 3-dimensional variations of closest packed arrangements to more open structures comprising 2-dimensional sheets or 1-dimensional chains.[1−3] Recently, there has been a growing interest in the development of qualitative structure maps for intermetallic compounds. This interest originates from the desire to develop new alloys with improved physical or mechanical properties or both.[4−7] The purpose of these maps is to separate structure types adopted by intermetallics with the use of parameters that have chemical significance. Such parameters can be atomic size, electronegativity, or valence electron count.

Some structure maps have been previously developed that do employ such parameters. For example, Villars uses the average valence electron count, the difference in the atomic radii, and the difference in electronegativity to construct 3-dimensional structure maps.[8,9] He examined 2-dimensional cross sections for a small range of average valence electron counts and found that compounds with the same first coordination sphere are generally located in the same region of the map.[10] Pettifor developed another type of structure map. His maps separate binary compounds through the use of two parameters: the Mendeleev number[11] and the stoichiometry of the A_nB_m compounds.[12] Compounds of a particular stoichiometry are mapped using the Mendeleev number of A versus the Mendeleev number of B. This parameter essentially numbers elements with the same valence electron count sequentially. Both of these structure maps achieve some success in separating intermetallic phases. However, neither of them uses the total electronic energy as a parameter for structure separation.

Although Hückel or tight-binding calculations have proven to be helpful in understanding structural changes,[13−16] the prediction of stability with the use of the total electronic energy as a guide has achieved limited success owing to what is referred as the coordination number problem.[17] In the past few years, a particular modification of the Hückel or tight-binding calculation has achieved surprising success in studying changes in structure as a function of changes in electron concentration (e^-/atom).[18−24] We applied this modification to intermetallics with the stoichiometry ZA_3 and ZA_6. Z is a more electropositive atom such as an element from groups I−V or a lanthanide, and A is a more electronegative atom such as a late transition metal or a main group element. The primary covalent bondings in these compounds are bonds between the A atoms. We will calculate the electron concentration (e^-/atom) using the Zintl concept for these compounds;[25−27] i.e. the more electropositive element, Z, is considered to donate its valence electrons to the covalent framework of the A atoms. The total energy is then calculated for only the covalent network of the A atoms.

Calculational Method: Second Moment Scaling

The modification of Hückel theory used in this study is known as second moment scaling. The second moment, μ_2, is defined as $\mu_2 =$

[†] Current address: Ames Laboratory, Iowa State University, Ames, IA 50011-3020.

[⊗] Abstract published in *Advance ACS Abstracts,* April 1, 1995.

(1) Villars, P.; Calvert, L. D. *Pearson's Handbook of Crystallographic Data for Intermetallic Phases,* 2nd ed.; American Society for Metals: Materials Park, OH, 1991.
(2) Daams, J. L. C.; Villars, P. *Atlas of Crystal Structure Types for Intermetallic Phases*; American Society for Metals: Newbury, OH, 1991.
(3) Pearson, W. B. *The Crystal Chemistry and Physics of Metals and Alloys*; Wiley-Interscience: New York, 1972.
(4) Lui, C. T. In *High-Temperature Alloys: Theory and Design*; Stiegler, J. O., Ed.; AIME: New York, 1984; p 289.
(5) Mooij, B.; Buschow, K. H. J. *Philips J. Res.* **1987**, *42*, 246.
(6) Pickett, W. E. *Rev. Mod. Phys.* **1989**, *61*, 433.
(7) A recent review of the interest in the relationship between electronic and geometric structure can be found in: *Bonding and Structure of Solids*; Haydock, R., Inglesfield, J. E., Pendry, J. B., Eds.; The Royal Society: London, 1991.
(8) Villars, P. *J. Less-Common Met.* **1986**, *119*, 175.
(9) Villars, P.; Hulliger, F. *J. Less-Common Met.* **1987**, *132*, 289.
(10) The first coordination sphere is found with the use of a graphing method developed by: Girgis, K.; Petter, W.; Pupp, G. *Acta Crystallogr.* **1975**, *B31*, 113.
(11) Pettifor, D. G. *Solid State Commun.* **1984**, *51*, 31.
(12) Pettifor, D. G. *J. Phys. C.: Solid State Phys.* **1986**, *19*, 285.
(13) Heilbronner, E.; Bock, H. *The HMO-Model and Its Applications*; Wiley: New York, 1976.
(14) Yates, K. *Hückel Molecular Orbital Theory*; Academic Press: New York, 1978.
(15) Burdett, J. K. *Prog. Solid State Chem.* **1984**, *15*, 173.
(16) Hoffmann, R. *Solids and Surfaces: A Chemist's View of Bonding in Extended Structures*; VCH Publishers: New York, 1988.
(17) Burdett, J. K. *Struct. Bonding* **1987**, *65*, 29.
(18) Pettifor, D. G.; Podloucky, R. *Phys. Rev. Lett.* **1984**, *53*, 1080.
(19) Burdett, J. K.; Lee, S. *J. Am. Chem. Soc.* **1985**, *107*, 3050.
(20) Cressoni, J. C.; Pettifor, D. G. *J. Phys.: Condens. Matter,* submitted for publication.
(21) Hoistad, L. M.; Lee, S. *J. Am. Chem. Soc.* **1991**, *113*, 8216.
(22) Lee, S. *Acc. Chem. Res.* **1991**, *24*, 249.
(23) Lee, S. *J. Am. Chem. Soc.* **1991**, *113*, 101.
(24) Lee, S. *J. Am. Chem. Soc.* **1991**, *113*, 8611.
(25) Zintl, E.; Goubeau, J.; Dullenkopf, W. *Z. Phys. Chem. (Leipzig)* **1931**, *154*, 1.
(26) Zintl, E.; Harder, A. *Z. Phys. Chem. (Leipzig)* **1931**, *154*, 47.
(27) Zintl, E.; Kaiser, H. *Z. Anorg. Allg. Chem.* **1933**, *211*, 113.

0020-1669/95/1334-2711$09.00/0

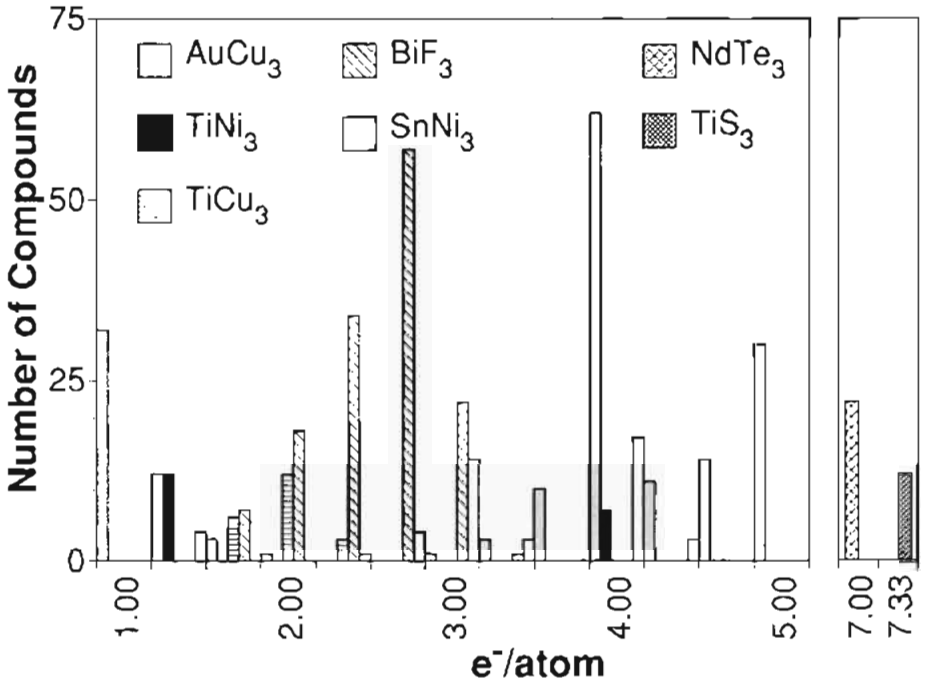

Figure 1. Number of known intermetallic phases as a function of electron concentration (e^-/atom) for the $AuCu_3$, $TiNi_3$, $TiCu_3$, BiF_3, $SnNi_3$, $NdTe_3$, and TiS_3 structure types.

$\sum E_i^2 = \sum(H_{ij}H_{ji})$ where E_i are the molecular orbital energies and H_{ij} are the elements of the Hamiltonian.[19,28-31] One term in this sum is a walk or hop from orbital i to orbital j. This walk is weighted by the interaction energy (H_{ij}) of orbitals i and j. The second portion of this term is a walk from orbital j back to orbital i. This sum is then taken over all orbitals in the structure. Hence, the second moment is an energetic measure of the average coordination of a particular structure. By scaling the second moments of two structures to be equal, we eliminate the effect of the differing coordination. After the second moments are scaled, the difference in total electronic energy between structures can then be directly compared.

The calculations performed in this study are of the simple Hückel type. We therefore solve the equation of $H\Psi = E\Psi$ instead of $H\Psi = ES\Psi$ as in extended Hückel theory.[13,14,16] The diagonal elements (H_{ii}) of the Hamiltonian are taken from the compendium of parameters.[32] The off-diagonal elements are calculated using the Wolfsberg–Helmholz approximation.[33] The second moments of all structures are fixed to a compound with one of the structure types considered in the study. The second moments are calculated using the formula $\mu_2 = \sum E_i^2$ where the orbital energies are calculated by the standard Hückel method in our band calculations. We continuously scale the density of each structure in an iterative fashion until the second moments are equal. The density is changed by expanding or contracting the cell parameters in a continuous manner.

Structural Chemistry of the ZA_3 Intermetallic Phases

There are nine major structure types with the stoichiometry ZA_3: $SnNi_3$, $TiCu_3$, $AuCu_3$, $TiNi_3$, TiS_3, $NdTe_3$, BiF_3, $ZrAl_3$, and $TiAl_3$.[34-42] Only those structure types adopted by at least 10 known compounds were considered as a major structure types. Figure 1 shows the number of compounds in each structure type as a function of electron concentration (e^-/atom). Some of these structure types have very narrow regions of stability (e.g. $TiCu_3$: 1.667–2.333). In contrast, other structure types are stable for wide range of electron concentrations (e.g. BiF_3: 1.667–3.333). $ZrAl_3$ and $TiAl_3$ are not included in this study since many of the compounds with these structure types are stable only at high temperature.[1] Since our calculational technique is valid only for systems at 0 K, we are currently unable to include these two structure types.

The ZA_3 intermetallics fall into two different structural groups: $SnNi_3$, $TiNi_3$, $AuCu_3$, $TiCu_3$, and BiF_3 are superstructures of face-centered cubic (fcc) or hexagonal closest packing (hcp) arrangements, while $NdTe_3$ and TiS_3 are structurally more open. Moreover, the two groups are stable at quite different electron concentration ranges (see Figure 1). The structures related to the closest packings, $SnNi_3$, $TiCu_3$, $AuCu_3$, $TiCu_3$, and BiF_3, are stable for low electron concentrations, near or below a half-filled s–p band. The structures of $NdTe_3$ and TiS_3 are stable for high electron concentrations, a nearly filled s–p band.

First we will discuss the structures of $NdTe_3$ and TiS_3. The compounds with these two structure types are generally chalcogenide phases. Figure 2 shows the network of the chalcogen atoms for these two structure types. In $NdTe_3$, two-thirds of the Te form square sheets of Te–Te bonded atoms. TheTe–Te bond distance in the square sheets is approximately 3.1 Å. These square sheets stack in double layers (Figure 2a). The

(28) Ducastelle, F.; Ducastelle, F. *J. Phys. Chem. Solids* **1970**, *31*, 1295.
(29) Ducastelle, F.; Cyrot-Lackmann, F. *J. Phys. Chem. Solids* **1971**, *32*, 285.
(30) Gaspard, J. P.; Cyrot-Lackmann, F. *J. Phys. C* **1973**, *6*, 3077.
(31) Burdett, J. K.; Lee, S. *J. Am. Chem. Soc.* **1985**, *107*, 3063.
(32) A compilation of extended Hückel parameters established mainly by the R. Hoffmann group at Cornell has been collected by S. Alvarez (University of Barcelona, 1987). This compilation is unpublished.
(33) The off-diagonal elements of the matrix are calculated with the use of the formula $H_{ij} = (k/2)S_{ij}(H_{ii} + H_{jj})$: Wolfsberg, M.; Helmholz, L. *J. Chem. Phys.* **1952**, *20*, 837.
(34) $SnNi_3$ ($TbCd_3$): Bruzzone, G.; Fornasini, M. L.; Merlo, F. *J. Less-Common Met.* **1973**, *30*, 361.
(35) $TiCu_3$: Raub, E.; Waler, P.; Engel, M. Z. *Z. Metallkd.* **1952**, *43*, 112.
(36) $AuCu_3$ ($DyIn_3$): Buschow, K. H. J.; de Wijn, H. W.; van Diepen, A. M. *J. Chem. Phys.* **1969**, *50*, 137.
(37) $TiNi_3$: van Vucht, J. H. N. *J. Less-Common Met.* **1966**, *11*, 308.
(38) TiS_3 ($HfTe_3$): Brattås, L.; Kjekshus, A. *Acta Chem. Scand.* **1972**, *26*, 3441.
(39) $NdTe_3$: Norling, B. K.; Steinfink, H. *Inorg. Chem.* **1966**, *5*, 1488.
(40) BiF_3 ($CeCd_3$): Tang, J.; Gschneider, K. A., Jr. *J. Less-Common Met.* **1989**, *49*, 341.
(41) $ZrAl_3$: Kematick, R. J.; Franzen, H. F. *J. Solid State Chem.* **1984**, *54*, 226.
(42) $TiAl_3$: Norby, P.; Christensen, A. N. *Acta Chem. Scand.* **1986**, *40A*, 157.

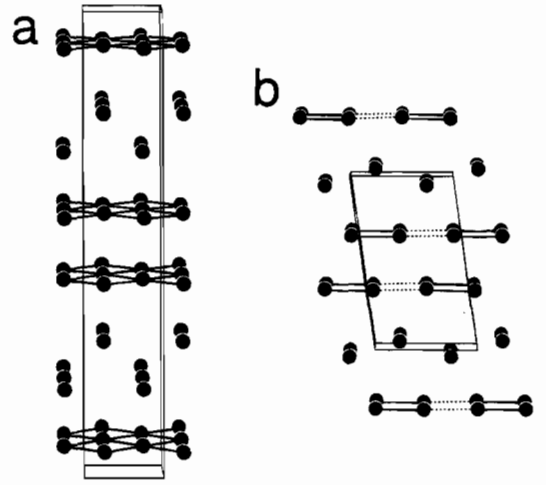

Figure 2. Structures of (a) $NdTe_3$ and (b) TiS_3. Only the chalcogen network is shown.

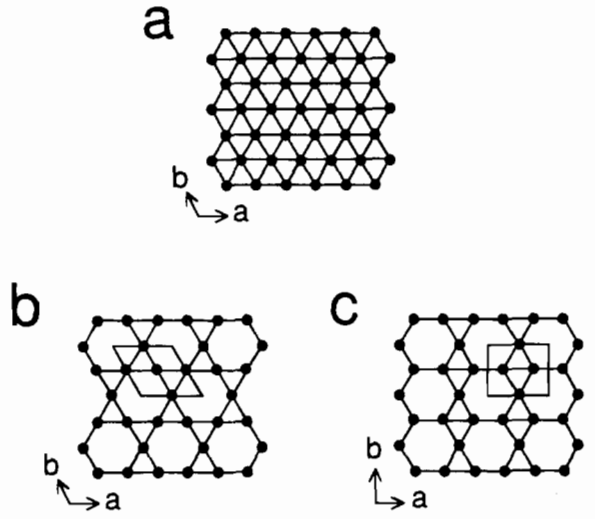

Figure 3. 2-Dimensional nets of atoms used in constructing (a) face-centered cubic and hexagonal closest packed arrangements, (b) $AuCu_3$, $SnNi_3$, and $TiNi_3$, and (c) $TiCu_3$.

other third of the chalcogen atoms lie between the double layers of square sheets. These latter atoms are 3.8 Å from their closest Te neighbor. Therefore, these atoms are considered isolated 2− anions. Finally, the cations are located in the layers with the 2− anions forming a distorted NaCl-type layer.

Closely related to $NdTe_3$ is the TiS_3 structure type (Figure 2b). As in $NdTe_3$, there are isolated 2− chalcogen anions which lie between double sheets of bonded chalcogen atoms. However, instead of square sheets, these atoms form chains. The bonds in the chains alternate in a short-long pattern. For example, in $ZrTe_3$, the short bond distances are 2.75 Å and the long bond distances are 3.13 Å. Distances between the chains are approximately 4.0Å.

$SnNi_3$, $TiCu_3$, $AuCu_3$, and $TiNi_3$ are superstructures of fcc and hcp.[34−37] Since these structure types are superstructures of closest packing arrangements, the framework of the A atoms can be described as a stacking of 2-dimensional layers of atoms. For each structure type, we will describe the 2-D nets and the stacking sequence of these nets. Parts b and c of Figure 3 show the 2-D layers found in $SnNi_3$, $TiNi_3$, $AuCu_3$, and $TiCu_3$. Both of these sheets are related to a 2-D closest packing of atoms shown in Figure 3a. The nets in Figure 3b,c are both formed by removing one-fourth of the atoms from the closest packed array. The defect pattern in Figure 3b retains the hexagonal symmetry of the closest packing and is commonly called a

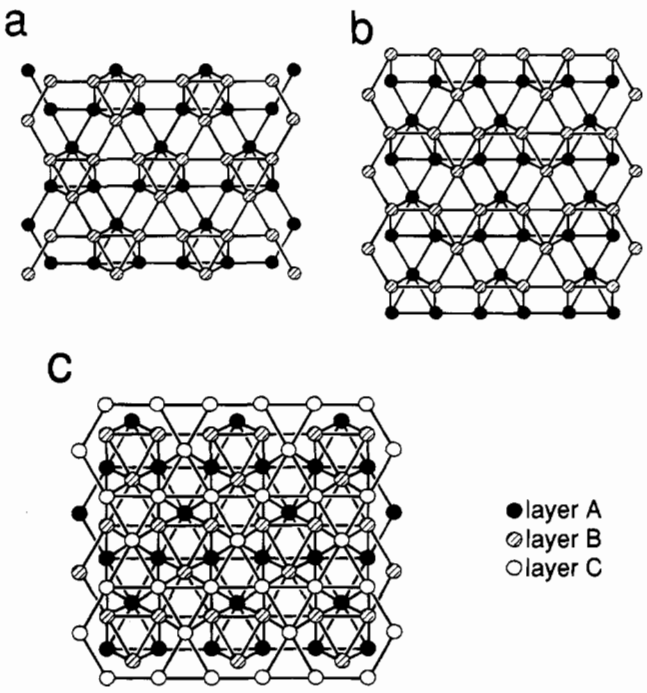

Figure 4. Structure types of (a) $SnNi_3$ ($TbCd_3$), (b) $TiCu_3$, and (c) $AuCu_3$ ($DyIn_3$). $SnNi_3$ and $TiCu_3$ are superstructures of hexagonal closest packing with the layers having an [AB] stacking sequence while $AuCu_3$ is a superstructure of face-centered cubic with an [ABC] stacking sequence.

kagomé net.[3] In contrast, the other defect pattern has a rectangular symmetry rather than hexagonal symmetry (Figure 3c). $SnNi_3$, $AuCu_3$, and $TiNi_3$ have stacked layers of the kagomé nets while $TiCu_3$ has stacked layers of the net with the rectangular unit cell.

As in hcp and fcc, $SnNi_3$, $TiCu_3$, $AuCu_3$, and $TiNi_3$ have stackings of the 2-D layers just described. Recall that a layer with a 2-D closest packing of atoms has two possible sites above which the atoms of the second layer can be placed. The repeat pattern of the layers determines the type of closest packing. Hexagonal closest packing produces an ABAB ... or [AB] stacking while fcc produces an ABCABC ... or [ABC] stacking. These same stacking sequences are found in $SnNi_3$, $TiCu_3$, and $AuCu_3$.

Figure 4 shows the structures of $SnNi_3$, $TiCu_3$, and $AuCu_3$. $SnNi_3$ and $TiCu_3$ have the same stacking pattern as hcp, [AB]. In $SnNi_3$, the atoms form columns of face-sharing octahedra in the stacking direction. $TiCu_3$ has stackings of the net with rectangular symmetry (Figure 3c). Instead of face-sharing octahedra as found in $SnNi_3$, the atoms form edge-sharing square pyramids. The $AuCu_3$ structure is an [ABC] stacking of kagomé nets. The structure contains vertex-sharing octahedra (Figure 4c). The Z cations in all of these structure types lie in the hexagonal holes of the 2-D layers, thus completing the closest packing of each layer (see Figure 3). The $AuCu_3$ structure can also be described as an ordered fcc arrangement. The cations are located on the vertices of the cubes while the anions are located on the face centers. $TiNi_3$ is another stacking variation using the kagomé net,[37] but it has an [ABAC] stacking repeat. This packing is intermediate between those of the $AuCu_3$ and $SnNi_3$ structures. Half of the layers (the "A" layers) have the $AuCu_3$ or fcc packing while the other half (the "B" and "C" layers) have the $SnNi_3$ or hcp packing. Compounds with these structure types have either late transition metals or early main group atoms forming the covalent network of atoms.

The BiF_3 structure type is also a variant of the face-centered cubic arrangement. Compounds with this structure type are

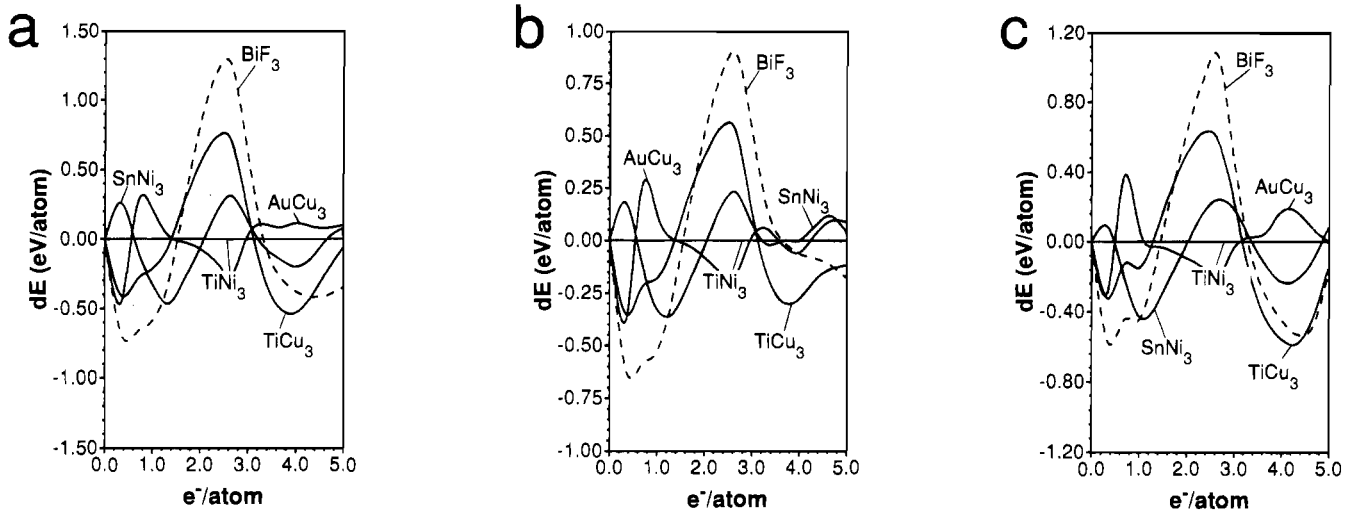

Figure 5. Difference in electronic energy per atom among $SnNi_3$, $AuCu_3$, $TiNi_3$, $TiCu_3$, and BiF_3 as a function of electrons per atom (e^-/atom). The convention of these curves is the following: the energy difference plotted is the difference with respect to the $TiNi_3$ structure. The curve which is most positive at a particular electron count is the most stable. Part a shows the energy difference derived from a 4s4p valence model and fitting all second moments to that of $TiCu_3$. Part b shows the energy difference derived from a 4s4p valence model and fitting all second moments to $ZrAu_3$. Part c shows the energy difference derived from a 6s6p valence model and fitting all second moments to $ZrAu_3$.

generally ternary phases of the composition ZAB_2.[1] The cation, Z, is usually a lanthanide. The A atoms are Al, Ga, or In and the B atoms come from either the Ni or the Cu triads. The cations themselves have an fcc packing. The A atoms fill the octahedral holes formed by the cations, and the B atoms fill all the tetrahedral holes. BiF_3 can thus be described as a stuffed fcc structure.

Structure Maps of the ZA_3 Intermetallic Phases

The analysis of the ZA_3 phases will be discussed in two parts. Recall that the two structural groups described earlier are very different from one another. $NdTe_3$ and TiS_3 are more open structures compared to the closest packed superstructures of $AuCu_3$, $SnNi_3$, $TiCu_3$, $TiNi_3$, and BiF_3 (Figures 2 and 4). In order to fit all the second moments to that of one structure type, the density of either group must be changed by a significant amount. For example, when all the second moments are fixed to that of $TiCu_3$, the bond distances of the isolated 2− anions in $NdTe_3$ are changed from 3.8 to 2.8 Å. This situation no longer reflects the true bonding character of $NdTe_3$. The drastic change in bond lengths makes it necessary to conduct the analysis in two parts: (i) the closest packed derivatives and (ii) TiS_3 and $NdTe_3$.

Closest Packed Superstructures. Compounds with the closest packed superstructures, $SnNi_3$, $TiNi_3$, $AuCu_3$, $TiCu_3$, and BiF_3, have both light and heavy elements comprising the covalent networks. Therefore, we calculated the energy of these structure types in three different ways. The first set of calculations used parameters which assumed a 4s4p valence state of the atoms.[43] The second moment for each structure type was fixed to that of $TiCu_3$. Thus the valence states of the compound match those of the Hückel parameters used. The second set of calculations used the same valence state for the parameters; however, we chose a compound containing a third-row metal, $ZrAu_3$ (also with the $TiCu_3$ structure type), as the reference to which the second moments were scaled. Finally, we used parameters with a 6s6p valence state and again scaled the second moments to $ZrAu_3$.[44,45] There is an increase in density of approximately 38% between $TiCu_3$ and $ZrAu_3$. Also, the observed ranges in electron concentration change when compounds contain light versus heavy elements. These calculations demonstrate the effect resulting from a change in the valence of the parameters and the density of compound used to fit the second moment.

Figure 5 shows the difference in energy for the $AuCu_3$, $SnNi_3$, $TiNi_3$, $TiCu_3$, and BiF_3 structure types as a function of electrons per atom for the three calculations mentioned above. Figure 5a shows the results from the calculation assuming a 4s4p valence state and fitting to the second moment of $TiCu_3$. Figure 6a compares the theoretical prediction to the experimental data. The experimental ranges have been modified from the ranges found in Figure 1. Instead of including all phases regardless of valence, the experimental ranges in this figure are only for those phases whose atoms are in a 3s3p or 4s4p valence state. The agreement between experiment and theory is quite reasonable for all phases except $SnNi_3$. Figure 5 shows that the $SnNi_3$ structure type would not be favorable in the region of 1.33−2.167 e^-/atom for any of the three calculations. $SnNi_3$ has primarily aluminum phases in the electron concentration range of 4−4.5 e^-/atom, whereas $AuCu_3$ has both aluminum and gallium phases at this electron count.[46] Some of the aluminides in this electron concentration adopt both the $AuCu_3$ and $SnNi_3$ structure types. Also, those compounds with the $SnNi_3$ structure type usually contain a rare earth metal that has less than a half-filled f shell whereas the aluminides with the $AuCu_3$ structure type have rare earth metals with more that a half-filled f shell. Since we are not including the electropositive element in our calculation, we cannot model this sort of effect. Aside from $SnNi_3$, the agreement is quite reasonable.

Figure 5b shows the energy difference for the calculation using 4s4p valence parameters and the fixing the second

(43) The parameters used for 4s and 4p valence states are taken from the literature for Ge: 4s, H_{ii} (eV) = −16.0, ζ = 2.16; 4p, H_{ii} = −9.0, ζ = 1.85. See: Thorn, D. L.; Hoffmann, R. *Inorg. Chem.* **1978**, *17*, 126.

(44) The parameters used for the 6s and 6p states is a combination of those for Au and Hg: 6s, H_{ii} = −16.07, ζ = 2.60; 6p, H_{ii} = −8.46, ζ = 2.58. Au: Komiya, S.; Albright, T. A.; Hoffmann, R.; Kochi, J. K. *J. Am. Chem. Soc.* **1977**, *99*.

(45) The Hückel parameters for Hg: Underwood, D. J.; Hoffmann, R.; Tatsumi, K.; Nakamura, A.; Yamamoto, Y. *J. Am. Chem. Soc.* **1985**, *107*, 5968.

(46) There is one compound with the $SnNi_3$ structure type which is not an aluminide and this is Ga_3Tb, which is also found in the $AuCu_3$ structure type.

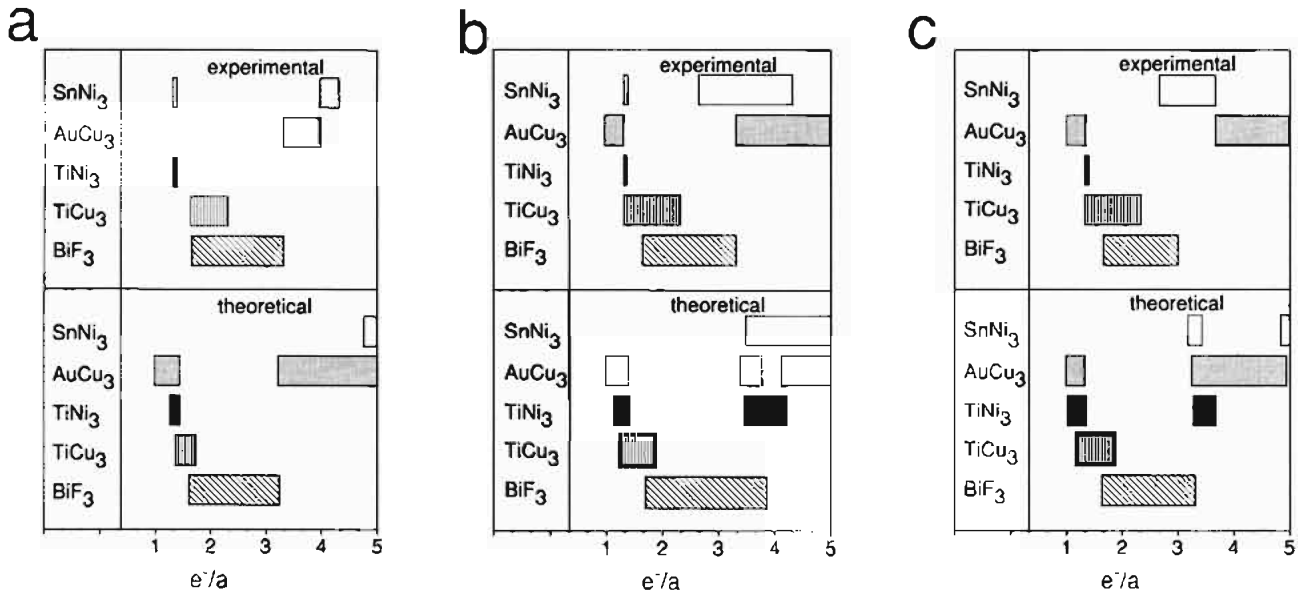

Figure 6. Comparison between the experimentally observed and the theoretically calculated ranges of electron concentration for $AuCu_3$, $SnNi_3$, $TiNi_3$, $TiCu_3$, and BiF_3. Part a shows the comparison between the calculation using a 4s4p valence model (see Figure 5a) and the compounds with atoms in a valence state of either 3s3p or 4s4p or both. Part b shows the comparison between the calculation in Figure 5b with all known phases regardless of valence. Part c shows the comparison between the calculation using the 6s6p valence model (see Figure 5c) and compounds with atoms in a valence state of either 5s5p or 6s6p or both.

moments to $ZrAu_3$. The shapes of the curves are essentially the same until an electron concentration of 3 e^-/atom is reached. Above 3.5 e^-/atom, there is essentially no difference in energy among $AuCu_3$, $SnNi_3$, and $TiNi_3$ structure types. The first-row parameters can no longer accurately model the bonding correctly because of the decrease in orbital overlap arising from the significant decrease in density.

Figure 5c shows the calculation using a 6s6p valence state, and the second moments are fixed to $ZrAu_3$. The comparison between the experimental data and the theoretical prediction is shown in Figure 6c. As with the 4s4p calculation, we only included experimentally found ranges with phases containing 5s5p and 6s6p valence states. We find that the agreement between the experimental data and our theoretical prediction is again quite good. This study illustrates the sensitivity of the parameters. It has been shown elsewhere that second moment scaling is a good model when one moves across a row of the periodic table.[24] By using the established Hückel parameters, we still have a problem studying changes directly as we move down a column. Therefore, in modeling intermetallic phases, some care must be taken in choosing parameters with the proper valency in order to achieve accurate results.

$NdTe_3$ and TiS_3. Figure 7 shows the difference in energy of the $NdTe_3$ and TiS_3 structure types. TiS_3 is stable at 7.33 e^-/atom while $NdTe_3$ is stable at 7e^-/atom (Figure 1). The agreement between theory and experiment is excellent. We may account for these results by means of a moments analysis.

A moment analysis associates structural features directly to the electronic energy. Earlier we defined the second moment. The general formula for the nth moment is $\mu_n = \sum(H_{ij}H_{jk}...H_{ni})$. As in the second moment, one term in this sum corresponds to the walks between overlapping orbitals.[19,28-31] These walks will be of length n and must begin and end with the same orbital. Certain structural features will have large contributions to the various moments. For example, structural features that strongly affect the third (μ_3) and fourth (μ_4) moments will be triangular and square arrangements of bonded atoms, respectively. Thus, the $AuCu_3$ structure type will have a large μ_3 since there are many bonded atoms in triangular arrangements in the structure. The $NdTe_3$ structure type will have a large μ_4 due to the square

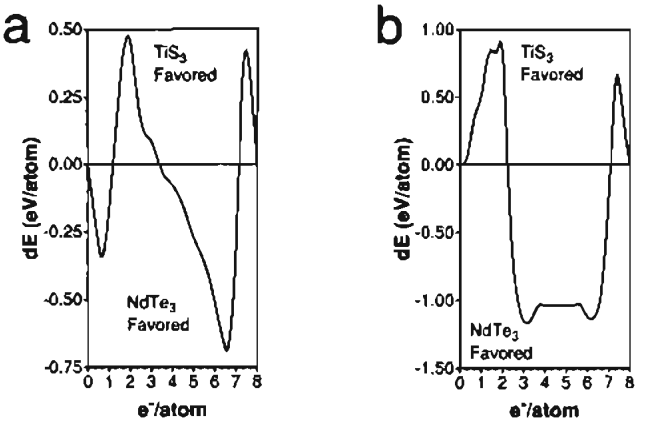

Figure 7. Difference in electronic energy between $NdTe_3$ and TiS_3 as a function of electrons per atom (a) when all chalcogen interactions are included in the calculation and (b) when chalcogen bonding interactions are limited to 3.5 Å (i.e., only the bonding interactions between atoms located in the chalcogen sheets are taken into account).

sheets of bonded chalcogen atoms. By examining these low moments, we can attribute the stability of these compounds to specific structural features.

As discussed earlier, the structural difference between the $NdTe_3$ and TiS_3 structure types is the sheets of bonded chalcogen atoms. In $NdTe_3$ the atoms form square sheets, but in TiS_3 they form chains with a short−long bond variation. Breaking the bonds of the $NdTe_3$ square sheets along one direction forms the chains found in TiS_3. This bond breaking makes a significant contribution to the fourth moment. At the band edges, structures with large fourth moments are stabilized while structures with small fourth moments are destabilized. However, the energy difference curve in Figure 7a shows an extra crossover at low band filling. This extra crossover arises from the isolated 2− anions between the sheets. Figure 7b shows the energy difference for the calculation where interactions between atoms is limited to 3.5 Å. Hence, only the first-nearest-neighbor interactions for the atoms in the chalcogen sheets are taken into account. The difference in energy now appears to be controlled by a fourth moment effect.

A moments analysis can confirm these results. In this analysis, we shall consider only the p orbitals involved in the σ-bonding of the sheet. **1** and **2** illustrate the relevant orbitals

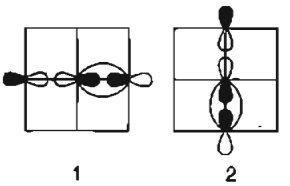

1 2

and the walks of length 2 for atoms in a square sheet. The walks must be between orbitals with a nonzero overlap, i.e. $H_{ij} \neq 0$. Hence, the walks can be only in either the x or the y direction. For this discussion, we assume that the H_{ij} for a walk from orbital i to orbital j is equal to β and that all bond lengths are equal. In $NdTe_3$, there are four unique walks of length 2 per atom in the square sheet. The second moment for $NdTe_3$ is $\mu_2 = 4(\beta\cdot\beta) = 4\beta^2$. In TiS_3, there are only two unique walks per atom since the bonds in the y direction are broken. Hence, the second moment for TiS_3 is $2\beta^2$. The second moment scaling technique requires that the two second moments be equal. We will set the second moments for the two structures equal to 1. Then the β's for $NdTe_3$ and TiS_3 are equal to $1/2$ and $1/\sqrt{2}$, respectively.

3 and **4** illustrate the walks of length 4 in the square sheet. Note that for each atom, there are three times as many unique

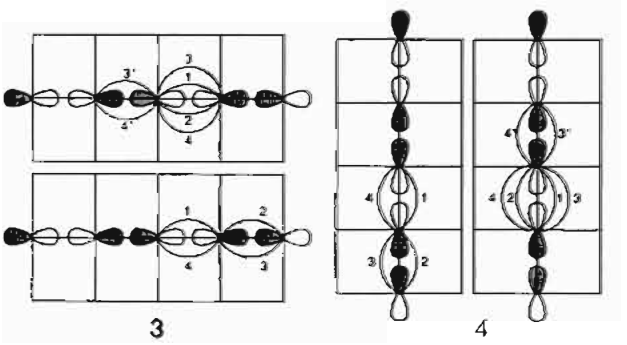

3 4

walks of length 4 in the x and y directions as there were walks of length 2. So the fourth moment is $12\beta^4$ for $NdTe_3$ and $6\beta^4$ for TiS_3. When the values for β calculated above after fixing the second moments are substituted, the fourth moment is 3/4 for $NdTe_3$ and 3/2 for TiS_3. These fourth moments suggest that TiS_3 should be more stable near the band edges while $NdTe_3$ should be less stable; this is in perfect agreement with experiment. A similar study for ZA_2 intermetallics also illustrated the importance of bond breaking in intermetallics with late main group atoms.[47] This moment analysis shows that the examination of the low moments is very useful for understanding the various structural features which stabilize these structure types at certain electron concentrations.

Compounds with ZA_6 Stoichiometry

There are only four major structure types with stoichiometry ZA_6: $SmAu_6$, $CeCu_6$, YCd_6, and $PuGa_6$.[48-51] For the ZA_6 phases, we considered major structure types to be those that have at least five known phases. Figure 8 shows the electron

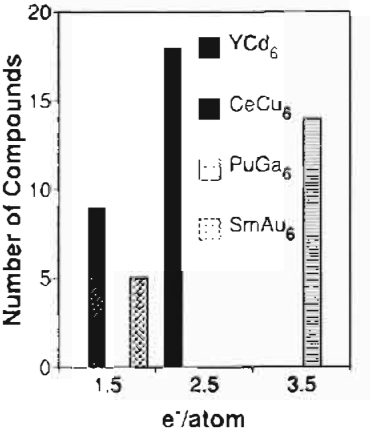

Figure 8. Number of compounds as a function of electron concentration (e^-/atom) for intermetallics with the stoichiometry of ZA_6.

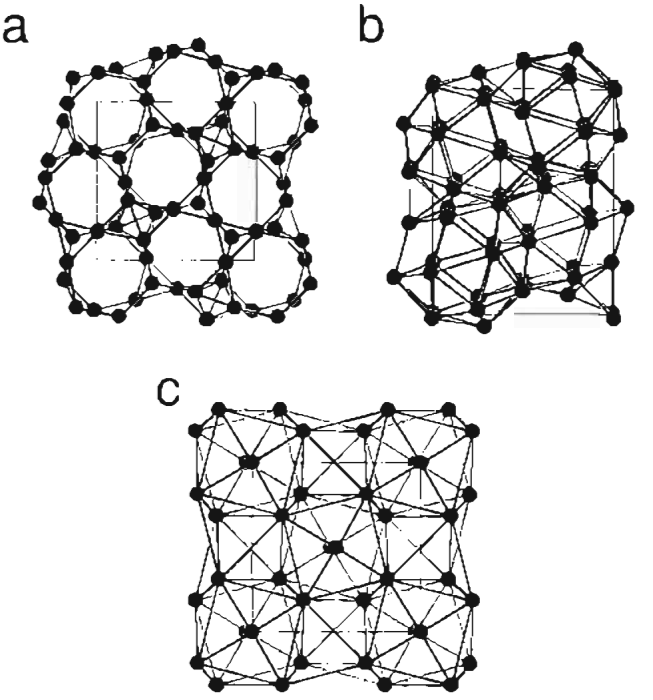

Figure 9. Structure types of (a) $SmAu_6$, (b) $CeCu_6$, and (c) $PuGa_6$.

concentration ranges for these structure types. Unlike the ZA_3 compounds, all the ZA_6 structure types are generally electron-precise compounds and are composed of only one electronegative atom type. For example, rare earth gold compounds have the $SmAu_6$ structure type, whereas rare earth copper compounds adopt the $CeCu_6$ structure type. In YCd_6, one Cd site has a $^1/_3$ occupancy. Since the true superstructure is not known, we will not include this structure in our study.

Figure 9 shows the structures of $SmAu_6$, $PuGa_6$, and $CeCu_6$. The $SmAu_6$ structure has layers of face-sharing hexagonal antiprisms. These antiprisms are capped above and below by Au atoms from the adjacent layers. The $CeCu_6$ structure type has large 19-vertex polyhedra which are again face-sharing, with tetrahedra filling the voids between polyhedra. These polyhedra have a five-membered ring followed by two six-membered rings. The five-membered ring and one six-membered ring are capped (Figure 9b). The $PuGa_6$ structure consists of 10-vertex polyhedra which are edge-sharing. The polyhedra are slightly

(47) Lee, S.; Hoistad, L. M.; Carter, S. T. *New J. Chem.* **1992**, *16*, 651.
(48) $SmAu_6$: Flack, H. D.; Moreau, J. M.; Parthé, E. *Acta Crystallogr.* **1974**, *B30*, 82.
(49) $CeCu_6$: Cromer, D. T.; Larson, A. C.; Roof, R. B., Jr. *Acta Crystallogr.* **1960**, *13*, 913.
(50) YCd_6: Larson, A. C.; Cromer, D. T. *Acta Crystallogr.* **1971**, *B27*, 1875.
(51) $PuGa_6$: Ellinger, F. H.; Zachariasen, W. H. *Acta Crystallogr.* **1965**, *19*, 281.

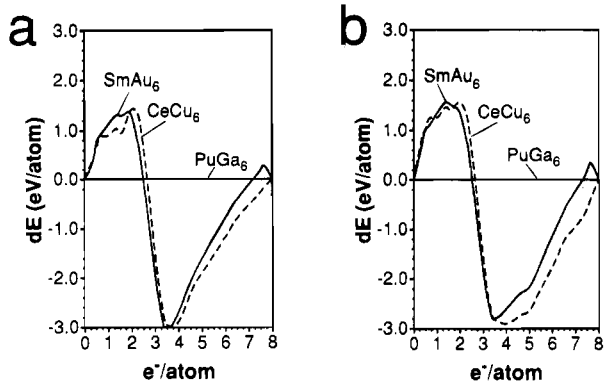

Figure 10. Difference in electronic energy among the structure types of $SmAu_6$, $CeCu_6$, and $PuGa_6$. Part a shows the difference when a 4s4p valence model is used, and Part b shows the difference when a 6s6p valence model is used.

twisted cubes which are capped on two ends. In all of these structures, the cations are located in the centers of the large polyhedra.

Figure 10 shows the energy difference curves for $CeCu_6$, $PuGa_6$, and $SmAu_6$. The results from calculations using Hückel parameters with a 4s4p valence state are shown in Figure 10a and with a 6s6p valence state in Figure 10b. With either set of parameters, $CeCu_6$ and $SmAu_6$ are better structural alternatives than $PuGa_6$ at 1.5 e^-/atom and $PuGa_6$ is the best structure at 3.5 e^-/atom. However, $SmAu_6$ is more stable that $CeCu_6$ for both sets of parameters.

The energy difference between $SmAu_6$ and $CeCu_6$ is quite small. Nevertheless, $SmAu_6$ is slightly more favorable than $CeCu_6$. Also, these compounds have nearly the same density, which was not the case in the ZA_3 phases where there is a significant increase in density between phases with a 4s4p versus a 6s6p valence state. In all the calculations presented, we have modeled only part of the total electronic energy, the covalent energy for the A−A interactions. The ionic portion of the energy has been completely ignored. The inclusion of the ionic interactions of the rare earth and the Cu or Au atoms may be able to account for the difference in correctly predicting $CeCu_6$ as the favored structure for elements in a 4s4p valence state instead of $SmAu_6$. There has been a recent study which does include an ionic term in order to rationalize the structural possibilities for rare earth selenide superstructures and which has been successful.[52]

Conclusion

We have shown that structure maps based on second moment scaled energies as a function of electron concentration can correctly model the stability of intermetallic compounds. Some consideration should be given to such effects as the size and the parameters chosen to model these phases. Agreement for phases found for similar electron concentration still requires further study as is the case for the ZA_6 intermetallics. There are some important energetic effects such as the ionic interactions which have been neglected but may play an important role for modeling of intermetallic phases.

Acknowledgment. I especially wish to thank Prof. Stephen Lee for invaluable discussions about this paper. The band program used in this study is a modified version of the program written by R. Hoffmann, M.-H. Whangbo, T. Hughbanks, S. Wijeyesekera, M. Kertesz, C. N. Wilker, and C. Zheng. I also wish to thank G. Miller for his irreducible wedge k-space programs, Dr. Jeff Kampf, who supplied unlimited use of his computing facilities, and the Rackham Graduate School and Petroleum Research Fund for partial support of this work.

Supplementary Material Available: Listings of the known intermetallic phases with the stoichiometries of ZA_3 and ZA_6 by structure type (6 pages). This material is contained in many libraries on microfiche, immediately follows this article in the microfilm version of the journal, and can be ordered from the American Chemical Society; see any current masthead page for ordering information.

IC9407510

(52) Lee, S.; Foran, B. *J. Am. Chem. Soc.* **1994**, *116*, 154.